APCC
APEC CLIMATE CENTER

TECHNICAL REPORT

APCC
APEC CLIMATE CENTER

PREFACE

It is our pleasure to present to you the APEC Climate Center (APCC)'s Technical Report 2012, which reports the core outcomes of our research activities from the past year.

Since 2005, APCC, as a hub of climate information in the Asia-Pacific region, has strived to share our analysis and prediction of abnormal climate and to apply this information to regional development. The Center has established the most extensive Multi-Model Ensemble (MME) system for seasonal prediction in the world through its international science network and has provided value-added products to various stakeholders. Recently, APCC has expanded its mandate to include enhancing the capacity of APEC member economies to respond effectively to climate change and variability through better application of climate information.

In 2012, APCC continued to make an effort to improve the quality and quantity of our short-term climate forecasts and our online climate information systems, as information dissemination tools. Additionally, APCC began its endeavor to produce more applicable climate information through interdisciplinary research among various sectors, such as agriculture and hydrology. The following technical report provides more information about our research outcomes from 2012.

In 2013, following APCC's goal to enhance socioeconomic well-being through better utilization of climate information, APCC will continue to improve the quality and accuracy of its climate information, recognizing that the utility of this information is only as good as its quality. We would like to make the best use of our research outcomes in various scientific and application areas. We welcome any feedback on this report or on our services.

My best and warmest regards to all of you.

Dr. Chin-Seung Chung
Director/APEC Climate Center

CONTENTS

APCC

TECHNICAL REPORT 2012-01

Decadal Change of Variability and Predictability of Two Types of ENSO

Ms. Hye-In Jeong

ABSTRACT

The forecast skill of a coupled multi-model ensemble (MME) in predicting two main types of the El Niño-Southern Oscillation (ENSO), (namely the canonical or "cold tongue" and the "warm pool" or El Niño Modoki), and their regional climate impacts, is assessed for the boreal winter. Based on a hindcast set of boreal winter predictions for the period 1972–1988 and 1989–2005, we show that the MME is able to predict and discern important differences between the canonical and warm pool ENSOs in the patterns of tropical Pacific sea surface temperature anomalies, 1 and 4 month ahead, for the two periods, respectively. The coupled MME predicts decadal changes of the distinct impacts of the canonical ENSO reasonably well, including the intensified winter monsoon rainfall over East Asia, the weakened below-normal rainfall over Australia, the strengthened anomalously wet conditions across the southern USA, and the anomalously dry conditions over South America. However, there are some limitations in the MME's ability to capture rainfall anomalies associated with the different types of ENSO for the early period, at a lead time of 1 and 4 months, particularly over the Indian Ocean, equatorial western and central Pacific. Nevertheless, the forecast skills for rainfall over East Asia during the different types of ENSO are comparable to, or slightly higher than, those during canonical ENSO events.

1. INTRODUCTION

1.1 Climate regime shift

Since the late 1970's, there has been a significant change in the tropical Pacific sea surface temperature (SST) and sea level pressure fields (Nitta and Yamada 1989; Trenberth and Hurrell 1994; Graham 1992, 1994). Since this time, and that the regime shift of SST has been characterized by an abrupt change toward a warmer tropical eastern Pacific and a colder extratropical central north Pacific since this time (Wang 1995; Zhang *et al.* 1997). Studies have emphasized the importance of this in relation to interdecadal climate variability over the north Pacific and North America (Trenberth and Hurrell 1994; Xie *et al.* 2010b; Wang *et al.* 2008; Lee *et al.* 2012).

Recent studies have provided evidence of other shifts, with particular attention focused onea that occurred during the winter of 1988/89 in the north Pacific basin climate (Hare and Mantua 2000; Hollowed *et al.* 2001; Yasunaka and Hanawa 2003). Hare and Mantua (2000) documented many coherent changes in biological variables

during the 1988–89 climate regime shift, and further argued that these changes were neither as prominent as they were in 1976/1977 nor did they signal a simple return to pre-1976/77 conditions throughout the north Pacific climate and marine ecosystem. It was discovered that a notable feature of the 1988/89 regime shift was its clarity in the biological records in contrast to the lack of clear changes expressed in the indices of the Pacific climate. Several studies have emphasized also that the large scale structure of decadal changes which occurred across the winter of 1988/89 have different characteristics from those of the winter of 1976/77 (Walsh *et al.* 1996; Tanaka *et al.* 1996; Watanabe and Nitta 1999), and that the shift in the North Pacific climate during the winter of 1988/89 differs from the shift in 1976/77 in terms of atmospheric circulation and associated surface climate variations (Yeh *et al.* 2011).

1.2 Two types of ENSO and their impacts

There has been a considerable amount of research into athe new type of ENSO, which hasve equivalently been referred to as “dateline” (Larkin and Harrison 2005b), “El Niño Modoki” (Ashok *et al.* 2007), “Central-Pacific” (Yu and Kao 2007; Kao and Yu 2009), and “Warm Pool El Niño” (Kug *et al.* 2009, 2010), in order to differentiate it from the typical El Niño that develops further east in the cold tongue of the equatorial Pacific, (such as that during 1997) (McPhaden 1999). A distinguishing factor of El Niño Modoki is that the maximum sea surface temperature anomaly (SSTA) occurs in the central equatorial Pacific rather than in the eastern Pacific, and the SSTA is typically flanked by cold anomalies further east and west, which last for several seasons. El Niño Modoki appears to be a recent phenomenon, with eight El Niño Modoki events occurring since the 1980s, including the recent El Niño Modoki event in 2009 (Ashok *et al.* 2007; Ratnam *et al.* 2010). (For reference, five canonical El Niño events, also known as “cold tongue El Niño” (Hendon *et al.* 2009) or “eastern Pacific El Niño” (Yu and Kao 2007) have occurred since 1980. Prior to the 1980’s no El Niño Modoki events were reported, although Donuy and Dessier (1983) and Fu et al (1986) discuss distinct characteristics of a few individual events. Anomalous warming in the central Pacific in the pre-1980s stemmed from the transient evolution of canonical El Niño events (e.g., Trenberth and Stepaniak 2001). Studies hint that

the recent frequent occurrences of El Niño Modoki are associated with recent climatic changes in the Pacific, in particular the flattening of the tropical Pacific thermocline in association with slackened trade easterlies (Ashok *et al.* 2007; Turner *et al.* 2007; Yeh *et al.* 2009). A flatter thermocline favors the generation of SST anomalies in the central Pacific via zonal advection and surface heat flux variations, as opposed to SST anomalies further east in the cold tongue that result from a vertical displacement of the thermocline and which typically occur in canonical El Niños (Kug *et al.* 2009; Yu and Kim 2010).

The climatic impact of Modoki and canonical El Niños, differ distinctly, particularly over East Asia, Australia, and the United States (e.g., Larkin and Harrison 2005a; Ashok *et al.* 2007, 2009a,b; Weng *et al.* 2007, 2009; Wang and Hendon 2007; Lim *et al.* 2009; Taschetto and England 2009; Trenberth and Smith 2009; Cai and Cowan 2009; Mo 2010; Pradhan *et al.* 2011). For example, during the boreal winter, El Niño Modoki events weaken the East Asian winter monsoon by shifting the low-level anticyclone to the South China Sea, whereas during canonical El Niño events the winter monsoon strengthens due to a shift of the anticyclones to the Philippine Sea (Weng *et al.* 2009). The Australian spring rainfall has the greatest sensitivity to the SST variations on the eastern edge of the Pacific warm pool area (Wang and Hendon 2007), and is thus more sensitive to El Niño Modoki events than those of canonical El Niños (Hendon *et al.* 2009; Lim *et al.* 2009). In contrast, however, Australian autumn rainfall is sensitive to El Niño Modoki (Cai and Cowan 2009).

Although the distinctive impacts of El Niño Modoki events have been well established, there has been little effort to assess the skill of the models in predicting them. Hendon *et al.* (2009) and Lim *et al.* (2009) showed limited success in predicting the differences between Modoki and canonical El Niños, using the Bureau of Meteorology POAMA coupled seasonal forecast model; the prediction skill was limited by a systematic model error whereby the POAMA model was unable to maintain the distinction between Modoki and canonical events beyond a lead time of about one season. To predict the distinctions between Modoki and canonical El Niños and their distinctive regional impacts in the boreal winter, Jeong *et al.* (2012) assessed the ability of the APCC Multi-Model Ensemble (MME) suite and found that it fairly

successfully predicted and discerned the important differences in the patterns of tropical Pacific SST anomalies between the two kinds of ENSOs, 1- and 4-months ahead, as well as predicting the distinct impacts of each reasonably well.

1.3 Objectives of this study

The present study aims to assess the ability to predict the decadal change of tropical Pacific SST variability and assess the ability to predict the associated regional climate impact changes. We identify how the seasonal predictability changes along with the tropical Pacific Ocean's climate shift and the decadal change of the ENSO characteristics in the late 1980s. Our strategy was to compare the seasonal predictability of six coupled ocean-atmosphere numerical models using the coupled climate prediction Multi-Model Ensemble (MME) approach, whereby systematic model errors should be averaged out. Here we focus on the 4-month lead (August 1 initial condition) and the 1-month lead (November 1 initial condition) prediction skill for the boreal winter, using hindcast data for two contrasting periods: before the tropical Pacific climate shift (1972 to 1988, hereinafter referred to as "PRE") and after the climate shift (1989 to 2005, hereinafter referred to as "POST").

Section 2 gives a brief description of the forecast data and MME methodology. In section 3, we examine the ability of the coupled MME to predict the decadal changes of two different types of ENSO events, and report the prediction skill related to the regional impacts of the two types of ENSO changes in the Asia-Pacific. The last sections comprise of a discussion and summary of this study.

2. METHODOLOGY

2.1 Data used

The data used in the present study are the seasonal retrospective forecast output from six coupled models. The six coupled models are from BoM in the Asia-Pacific Economic Cooperation Climate Center/Climate Prediction and its Application to Society (APCC/CliPAS) (Wang *et al.* 2009; Lee *et al.* 2010) and from CMCC-INGV, ECMWF, IFM-GEOMAR, MF, and UKMO in the ENSEMBLE-based predictions of climate changes and their impactS (ENSEMBLES) project (Weisheimer *et al.* 2009). None of the coupled models has flux adjustment. A brief description of the models is provided in Table 1.

In this study, we form the multi-model ensemble using the simple composite method (Peng *et al.*, 2002; Kang *et al.*, 2009; Lee *et al.*, 2008, 2009, 2011). With this technique, equal weights are assigned to the ensemble mean predictions of each model, with the assumption that each model is independent. The mean bias from each model is removed by forming anomalies with respect to the each model's own seasonal climatology. In this study, we focus on the boreal winter (December through February; "DJF") for the period of 1972–2005. We used hindcasts of 6 selected models for DJF using the initial condition of 1 November, (1-month lead seasonal prediction), and hindcasts with the initial condition of 1 August (4-month lead seasonal prediction), to investigate the seasonal predictability from the initial condition as well as from the air-sea interaction.

The observed and reanalyzed datasets used for hindcast verification are the NOAA's PREC[1)] (Chen *et al.* 2002), the National Centers for Environmental Prediction (NCEP)-Department of Energy (DOE) reanalysis 1 data (Kalnay *et al.* 1996) for atmospheric variables, and the Extended Reconstructed Sea Surface Temperature (ERSST.v3b) data (Smith *et al.* 2008), for the period 1972–2005.

1) NOAA's PREC stands for NOAA's Precipitation Reconstruction (PREC)

Table 1 Description of one-tier prediction models used in this study

Institutes (model name)	AGCM (resolution)	OGCM (resolution)	Ensemble member	References
ECMWF (ECMF)	IFSCY31R1 (T159L62)	HOPE (0.3° × 1.4° L29)	9	Stockdale *et al.* 2011 Balmaseda *et al.* 2008
UKMO (EGRR)	HadGEM2-A (N96L38)	HadGEM2-O (0.33°lat × 1°lon L20)	9	Collins *et al.* 2008
MF (LFPW)	ARPEGE4.6 (T63L31)	OPA8.2 (2°lat × 2°lon L31)	9	Daget *et al.* 2009 Salas Melia, 2002
IFM/GEOMAR (IFMK)	ECHAM5 (T63L31)	MPI-OMI (1.5°lat × 1.5°lon L40)	9	Keenlyside *et al.* 2005 Ungclaus *et al.* 2006
CMCC-INGV (INGV)	ECHAM5 (T63L19)	OPA8.2 (2°lat × 2°lon L31)	9	Alessandri *et al.* 2011
BoM (P24A)	BAMv3.0d (T47L17)	ACOM2 (0.5°–1.5°lat × 2°lon 25)	11	Zhong *et al.* 2005

Table 2 Acronym names of institutions and models used in the text

Acronym	Full name
APCC	Asia-Pacific Economic Cooperation Climate Center
CMCC-INGV	Climate Prediction and its Application to Society
ECMWF	European Centre for Medium-Range Weather Forecast
ENSEMBLES	ENSEMBLE-based predictions of climate changes and their impactS
IFM-GEOMAR	Leibniz Institute of Marine Sciences at Kiel University
MF	Meteo France
POAMA	Predictive Ocean Atmosphere Model for Australia
UKMO	UK Met Office
ERSST	Extended Reconstructed Sea Surface Temperature
PREC	PRECipitation REConstruction Dataset

2.2 Evaluation methods

We first compared the climatological mean of sea surface temperature for 17 years in the two periods of PRE (1972–1988) and POST (1989–2005). We also examined the variance changes for SST and rainfall variability for the two periods. We then carried out an Empirical Orthogonal Function (EOF) analysis to identify the observed dominant spatial patterns of SST anomalies in the tropical Pacific. The teleconnection patterns were then extracted using a linear regression analysis of observed rainfall on the principal components of the top two EOF modes, which

represent the canonical and Modoki ENSO (Ashok *et al.* 2007). In order to examine the skill in predicting these observed features, we carried out similar analyses on the hindcasts of the MME. Pattern correlations were then employed to investigate the relationship between the observations and the coupled MME predictions for rainfall, in various regions surrounding the Pacific.

3. RESULTS

3.1 Changes in mean and variance

To assess the general capability of the MME in simulating and predicting seasonal mean climate features, we first compared the seasonal mean and differences for the two periods. The climatological winter (DJF) mean sea surface temperatures (SST) of the observed and predicted SSTs for the POST period of 1989–2005 and the climatological differences between POST (1989–2005) and PRE (1972–1988) for their observed and 1-month MME predictions are presented in Figure 1. The SST spatial pattern of the MME predictions matches the observed features reasonably well, in terms of the meridional SST gradients in the middle latitudes in both hemispheres, and the asymmetrical SST patterns in the east and west tropical Pacific. The cold bias of SST over the equatorial eastern Pacific, which frequently exists in individual coupled models, is much reduced (figures not shown). When mapping the difference between the two periods for the observed SST climatology, there is a noticeable warming trend during the POST period, especially in the Indian, Atlantic, and west Pacific oceans. The MME prediction successfully captures the warming trend over most regions in the northern hemisphere; however, there are significantly warm biases over the Arctic Sea in comparison with the observation. The 4-month lead MME prediction also successfully captures the major climatological features and the climate changes for the two periods, at a similar level of a 1-month MME prediction skill (Figures not shown).

To check the changes in variability for the two periods, we present the variance of SST and rainfall for the POST period and the variance ratio of POST to PRE for

observed and predicted SST and rainfall in Figures 2 and 3, respectively. The areas of maximum SST variability over equatorial eastern Pacific are well captured in the 1-month lead MME prediction, but the magnitude is slightly overestimated compared with that of the observation (Figure 2(c)). In the variance ratio of the two periods, The MME shows a weaker variability over the eastern Pacific and Indian Ocean in the observation and in the POST period (Figure 2(b)). The SSTA variability is slightly increased in the POST period over the western Pacific, but the ratio of variation is not significant. The coupled MME prediction at a 1-month lead time successfully captures the major changes in the weaker and stronger variability over the Tropics; however, the magnitude of the variance ratio is excessively represented. In the 4-month lead predictions, the MME has limitations in predicting the major changes of SST variability, indicating that maximum variability shifted to the western Pacific (figures not shown).

Figure 3 represents the variance of rainfall for the POST period and the variance ratio between the two periods of observed and predicted rainfall variability. The MME prediction at a 1-month lead time successfully simulated the variability of rainfall for the POST period over the tropical Pacific, in terms of representing the maximum variability over the dateline (180E, 10S–10N). However, the 1-month lead MME prediction had limitations in predicting rainfall variability precisely over land areas, and showed low variability over tropical South America (including Brazil), north Australia, and southern east Africa (Figure 3(c)). The 4-month lead MME prediction also had a similar problem with the 1-month lead prediction over land area (figures not shown). In the variance ratio of POST and PRE periods, the POST periods showed significantly much more variance in the observation, at the equatorial central and the western Pacific. Apart from in the tropical Pacific region, the rainfall variability is reduced in the POST period compared with that of the PRE. The rainfall variability is significantly reduced over eastern Australia in the POST period (Figure 3(b)). The MME prediction at a 1-month lead time also successfully captures the positive rainfall variance over the central Pacific; however, it simulates significantly low variability over Western Australia (Figure 3(d)). The 4-month lead MME prediction captures the positive variance over the equatorial eastern Pacific, but the magnitude is much reduced compared with that of 1-month lead MME prediction (figures not shown).

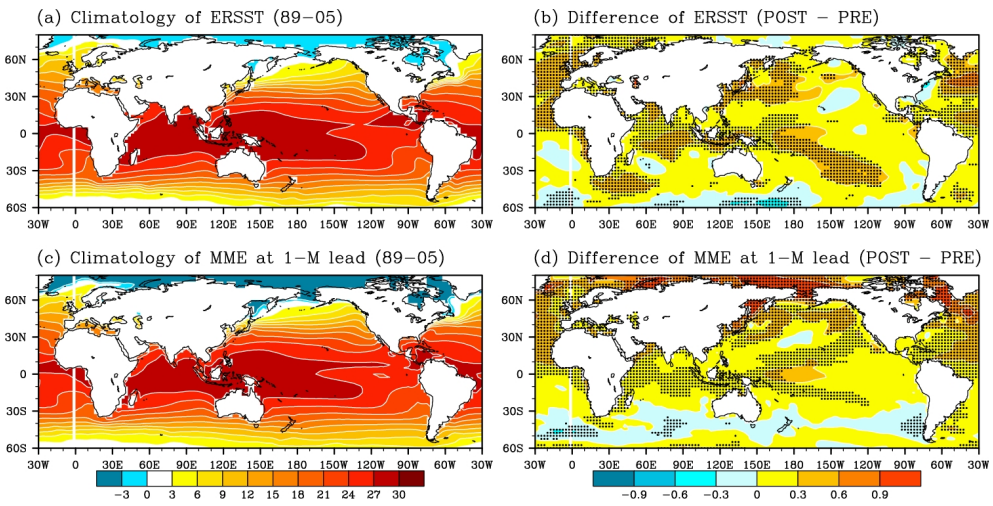

Figure 1 Climatological mean sea surface temperature (°C) for the period 1989–2005 in observed (a) and predicted (c) one-month lead MME; and climatological differences between 1989–2005 (POST) and 1972–1988 (PRE) for their observed SST (b) and one-month lead (d) MME predictions. The stippled areas denote the region where the statistical significance is above the 95% confidence level based on a Student's t-test.

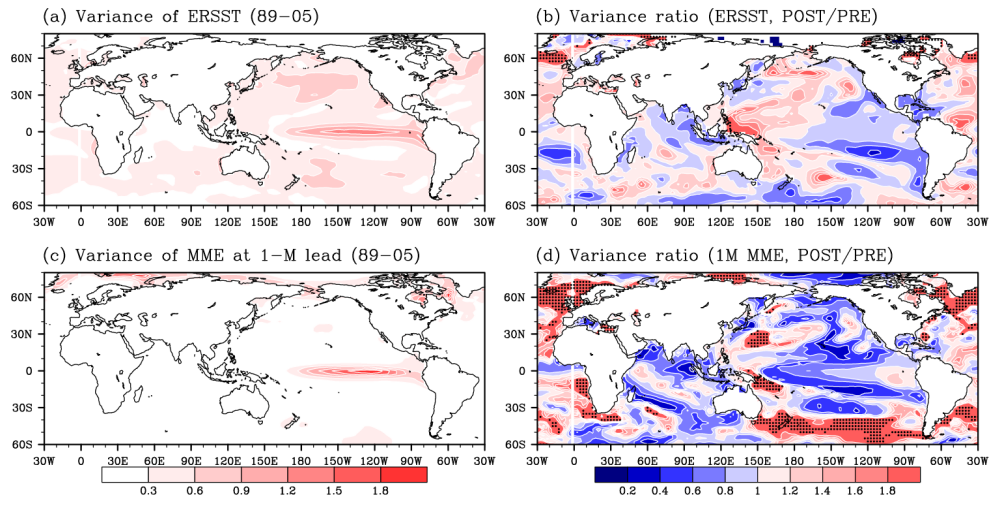

Figure 2 Variance of sea surface temperature (°C) for the period 1989–2005 in observed (a) and predicted (c) one-month lead MME and variance ratio of POST to PRE for their observed (b) and one-month (d) MME prediction.

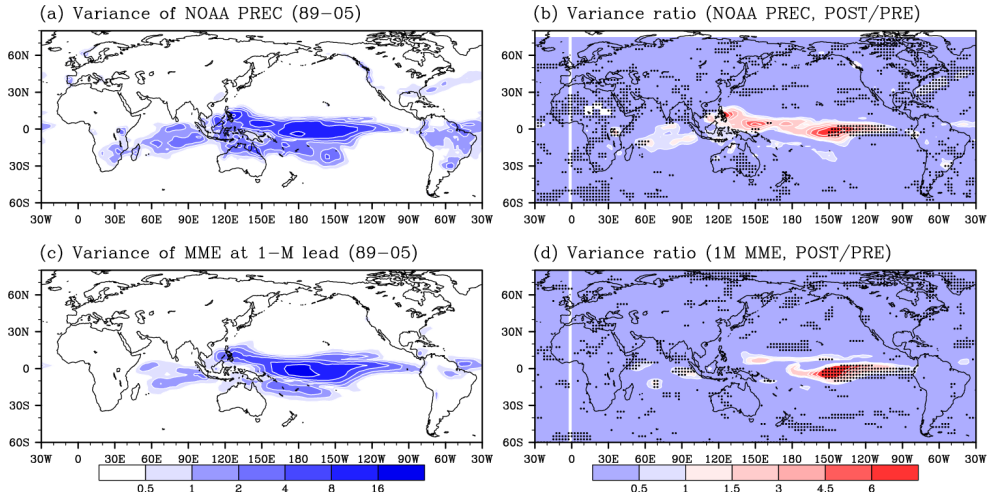

Figure 3 Same as Figure 2, but representing rainfall.

3.2 Changes in the major mode

Changes for the first EOF mode of tropical SSTA variability

The first leading mode of the observed SSTA during DJF over the tropical Pacific region (30S–30N, 120E–60W) for the two periods is presented in Figure 4(a) and 4(b). The spatial patterns of the first EOF mode (EOF1) captures the well-known canonical ENSO patterns with the SSTA retaining the same sign throughout the equatorial eastern Pacific and with the maximum occurring at about 155W–115W during both periods (Figure 4(a), 4(b)). The EOF1 explains the variability approximately 67.9% (56.9%) for the PRE (POST) period. The percentage variance for the POST period has been reduced by about 11% in comparison with the PRE period. However, the maximum SSTA variability over the equatorial eastern Pacific at around 155W–115W for the POST period, has been strengthened.

The ability of the MME to capture the canonical ENSO mode is assessed by performing a similar EOF analysis on the MME hindcasts at 1-month and 4-month lead times. The MME succeeds in capturing the spatial patterns of the first EOF modes at a 1-month lead time, with high fidelity (Figure 4(c), 4(d)). The correlation

of the spatial patterns between the observed and predicted eigenvectors is 0.94 for the PRE and POST period. However, the variances explained by the EOF1 for the MME are 79.4% and 72.9% (PRE and POST periods, respectively), indicating that the MME prediction explains a significantly larger amount of the variance than its observed counterpart.

At a 4-month lead, the MME is seen to more or less retain the high fidelity in capturing the spatial pattern of the EOF1 (Figure 4(e), 4(f)). The spatial pattern correlation between the observed and predicted eigenvectors is 0.94 and 0.93 for the two periods, slightly less than the corresponding value at a 1-month lead for the POST period (Figure 4(f)). The 4-month lead MME predictions have further increased the explained variance for the two periods.

The time series of the corresponding normalized PC1 for both the 1- and 4-month lead times for the two periods are presented in Figure 4(g) and, 4(h). The PC1 from observations is well correlated at 0.97 (0.96) with that of the MME hindcasts, at a 1-month lead for the PRE (POST) period. These correlations are statistically significant at a 99% confidence level using the two-tailed Student's t-test. It can be discerned that the MME successfully predicts both the spatial structure and the temporal behavior of the first EOF of SST. At a 4-month lead, the PC1 from observations is correlated at 0.92 with that from the MME hindcasts for the two periods. Even at a 4-month lead time, the correlations are statistically significant at 99% confidence level from two-tailed Student's t-test.

Changes for the second EOF mode of tropical SSTA variability

The second EOF mode (EOF2) of the observed SSTA during DJF over the same domain as shown in Figure 4(a), is presented in Figure 5(a) and 5(b) for the two periods. The second EOF mode of tropical SSTA in the POST period shows the maximum variability to be near the dateline, and is flanked by opposite signed anomalies in the far eastern and far western Pacific (Figure 5(b)). The EOF2 for the POST period is associated with ENSO Modoki mode (Ashok et al 2007; Hendon *et al.* 2009). However, in the PRE period, the EOF2 does not show any clear maximum variance in the

central tropical Pacific, and bears a visible resemblance to an ENSO developing features of La Niña. Ashok *et al.* (2007) compared the tropical SSTA variability before and after 1979. Their study also shows that the ENSO Modoki mode is not represented in the second EOF mode before 1979, and claims that the ENSO Modoki mode only appears in the current climate after 1979. The second mode explains 9.1% (16.9%) of the variance for the PRE (POST) period. Unlike the first mode of EOF analysis, the percentage variance of the second mode for the PRE period has been increased by 7.8% of the total variance.

The MME predictions at a 1-month lead time also successfully capture the second EOF mode, showing a high spatial pattern correlation of 0.83(0.88) for the two periods. The explained variance also increases during the POST period, but it again shows much less explained variance compared with that of the observation.

In the 4-month lead time, the spatial pattern correlations between the observed and predicted eigenvectors are 0.81 and 0.77 for the two periods, slightly less than the corresponding values in the 1-month lead. The spatial pattern of the EOF2 for the POST period indicates a strengthened central tropical Pacific loading and a weakened eastern equatorial Pacific variability, compared with that of the observation. The variance explained by the EOF2 from the MME has further reduced to 6.3% and 7.7% for the PRE and POST periods, respectively.

The PC2 from observations is correlated at 0.73 (0.65) with that of the MME hindcasts at 1- and 4-month lead times for the PRE period. For the POST period, the temporal correlation of PC2 has been increased to 0.90 (0.80) in the MME predictions with 1- and 4-month lead times. Even at a 4-month lead time, the correlations are statistically significant at 99% confidence level from two-tailed Student's t-test.

Performance of individual models in discerning tropical SSTA variability

We examined the performance of individual models for the dominant spatial patterns and temporal behavior of the first two leading EOF modes of the SSTAs

at 1- and 4-month lead times for the two periods in Figure 6, and compared the results with those of the MME predictions. Though the prediction skill of some individual models is slightly higher than that of the MME (especially, temporal correlations of PC2 in Figure 6(a) and (b)), it can be seen that overall, the skill of the MME in the spatial (temporal) correlation of the EOF2 pattern (PC2 time series) of SST anomalies at 1- and 4-month leads, is superior to the skill of individual models, as well as superior to the mean skill of individual models. In the POST period, the skill of the second EOF mode of the SSTA is increased compared to those of the PRE period, in all individual models and in the MME predictions. However, for the first EOF mode of SSTA, the temporal and spatial skills are robust for two periods even at a 4-month lead.

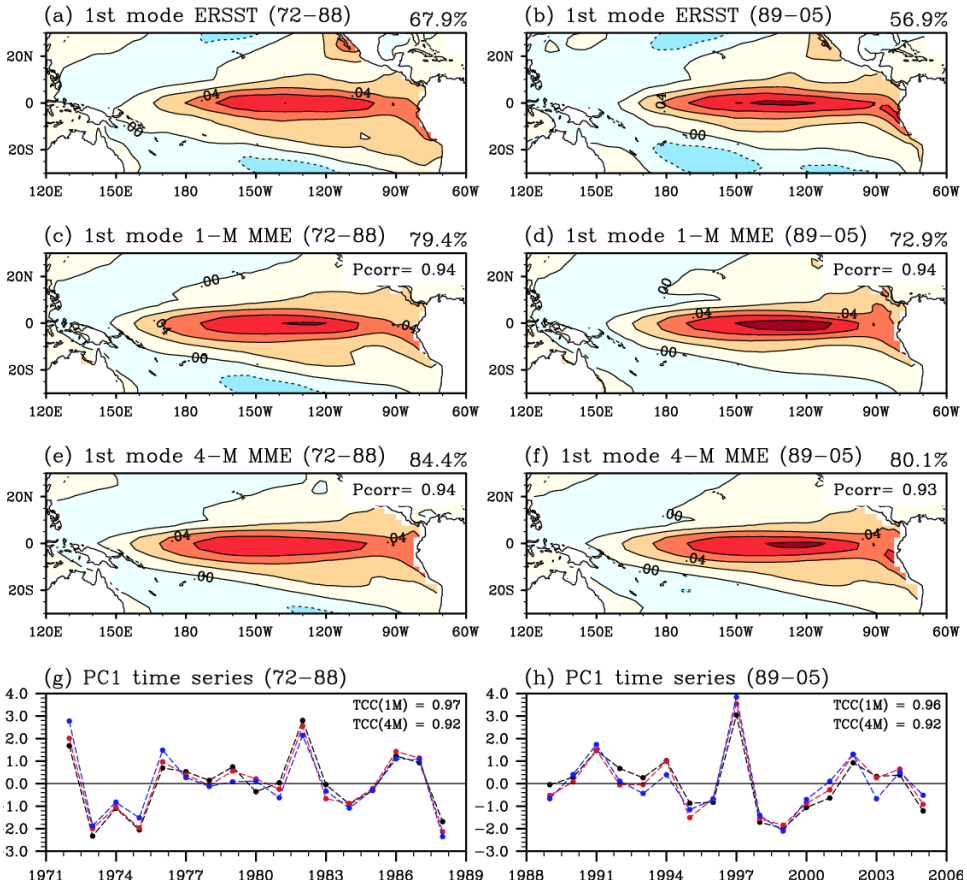

Figure 4 First modes of spatial patterns of EOFs for observed sea surface temperature anomalies over the tropical Pacific (30S–30N, 120E–60W) during the period of (a) 1972–1988 and (b) 1989–2005. (c) and (d) are the same as (a)and (b), except for the MME predicted sea surface temperature anomalies at a 1-month lead time. Pattern correlations between the observed and MME predicted spatial patterns of each EOF mode are also given. (e) and (f) are the same as (c) and (d) respectively, but at a 4-month lead time. Principal component (PCs) time series of the first EOF modes of sea surface temperature anomalies during the period of (g) 1972–1988 and (h) 1989–2005 from the observation (black), from the 1-month lead time MME predictions (red) and from the 4-month lead time MME predictions (blue). Time series are normalized by their respective standard deviation. Temporal correlations between observed and MME predicted PC1 time series are also given.

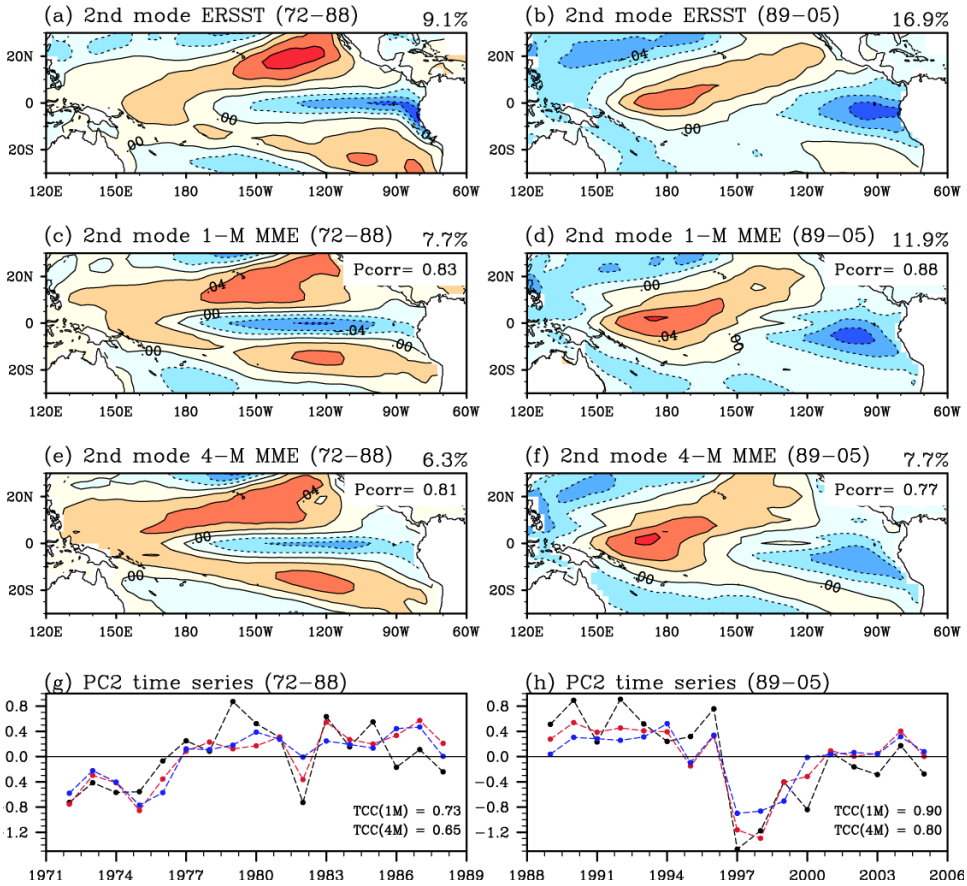

Figure 5 Same as Figure 4, but representing the second EOF modes.

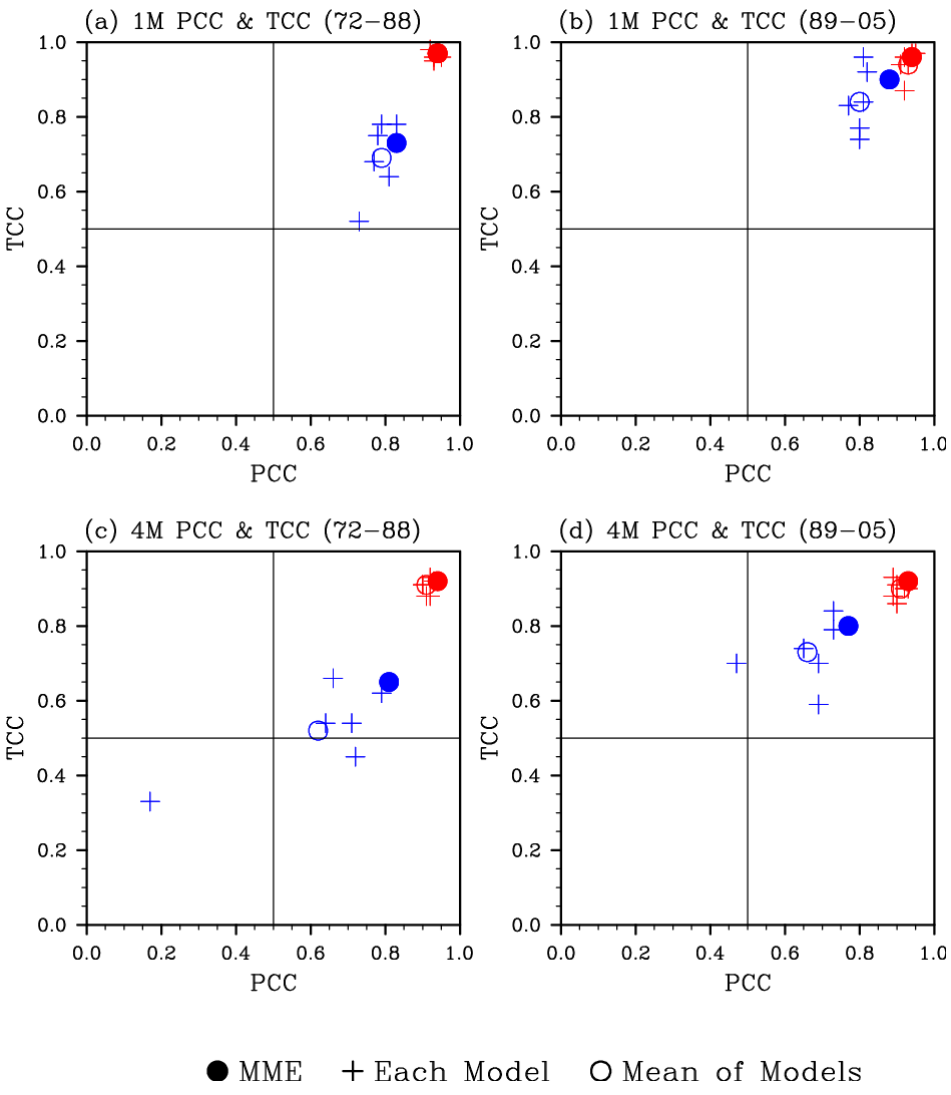

Figure 6 Distribution of the performance of the MME; individual models against the first two observed EOF modes of SSTAs over the tropical Pacific (30S–30N, 120E–60W) during the period of 1972–1988 (a) and (c) and 1989–2005 (b) and (d). The y-axis represents the temporal correlation coefficients of the corresponding principal components. The x-axis represents the pattern correlation coefficients of the eigenvector. The skills for the first mode (second mode) are denoted with red (blue). (a) and (b) are for the 1-month lead prediction skills and (c) and (d) are for the 4-month lead.

3.3 Regional impact by major mode changes

As shown in the previous section, the MME predictions at 1- and 4-month lead times is able to capture the first two leading modes of tropical Pacific SSTA variability. In this section, we briefly revisit the distinctive impacts of the two types of ENSO around the Pacific Rim, and examine how the coupled MME performs in predicting the observed impacts.

Remote climate associated with the first EOF mode over the tropical Pacific SST variability

Figure 7 shows the relationships between rainfall and SST variability which are the first leading EOFs of tropical Pacific SST variability are demonstrated by regressing the observed SSTA on to the standardized PC1 (Figures 4(e) and 5(e)), for the two periods. During a canonical El Niño (Figure 7(a),(b)), positive rainfall anomalies are observed over ITCZ in the eastern and central Pacific, flanked to the west by a broad horse-shoe shaped negative rainfall anomaly centered in the western tropical Pacific that extends eastward into the northern and southern Pacific. Anomalously dry conditions are seen in the SPCZ, Maritime Continent, western tropical Pacific and the Philippines (in agreement with Weng *et al.* 2009). Drought conditions exist over tropical South America. Such below normal rainfall conditions are shown in both the PRE and POST periods, and this unique feature is already documented in earlier studies, (Ropelewski and Halpert (1987, 1989); Diaz *et al.* (2001); Saji and Yamagata (2003), and Ashok *et al.* (2007)). An anomalous dry condition is seen over most of Australia in the PRE period, and is more significant in eastern and northern Australia. However, during the POST period, the anomalous dry condition over Australia is weakened, and instead shows positive rainfall anomalies over eastern Australia. During the POST period, there is also an anomalously strong and intensified winter monsoon rain band over the southern part of North America, into the North Atlantic Ocean and over most areas of the Indian Ocean (Figure 7(b)).

We then assessed how well the MME predicted the aforementioned rainfall features associated with the first two leading modes of tropical SST variability, by carrying out a regression analysis similar to that for the observations. The regression pattern of the hindcast rainfall onto PC1 at a 1-month (4-month) lead time for the two periods is shown in Figure 7(c)(d) and 7(e),(f). In general, the MME prediction replicates the observed features well. For example, the anomalously strong monsoon rainfall in East Asia and the anomalously wet (dry) conditions over North (tropical South) America are well represented for the two periods. However, the unrealistic anomalously wet conditions over the equatorial maritime continents and equatorial eastern Pacific in the 1- and 4-month MME predictions, which were attributed to a systematic model bias in the representation of the canonical El Niño, are in the intrinsic mode of all of the individual coupled models (in agreement with Jeong *et al.*, 2012). At a 4-month lead time, the regression patterns of rainfall are very similar to those of a 1-month lead time. The dipole mode that shows wet and dry conditions over the Indian Ocean is a predominant feature, and the whole of Australia shows anomalously dry conditions. The MME predictions at a 1- and 4-month lead successfully capture the intensified rainfall anomalies over the southern part of North America for the POST period.

Remote climate associated with the second EOF mode over the tropical Pacific SST variability

Figure 8 shows the relationships between rainfall variability with the second EOFs of tropical Pacific SST variability demonstrated by regressing the observed SSTA on to the standardized PC2 (Figures 4(f) and 5(f)), for the two periods. Positive rainfall anomalies over the western tropical Pacific including the Maritime continents, Western Australia and the Philippines are observed in the PRE period, and there are other positive rainfall anomalies over the ocean adjoining Polynesia at around 150W, 20S. Dry conditions exist over the Indian Ocean, but these are not significant. However, unlike the PRE period, the POST period reveals anomalously wet (dry) conditions to the west of the dateline (equatorial eastern Pacific). A point of specific interest is that the signs are completely different in the POST and PRE periods the

Indian Ocean, the western Pacific (including Maritime continents), and Australia. During the POST period (ENSO Modoki), the winter monsoon in central eastern China is anomalously weak, whereas it is quite strong during canonical El Niño (Figure 7(b)). The anomalous rainfall associated with the two tropical Pacific phenomena during the POST period, is also opposite to one another in East Asia. These findings agree with Weng *et al.* (2009).

The observed triple mode of anomalously dry, wet, and dry conditions over the equatorial central Pacific associated with the second EOF mode is well predicted retrospectively by the 1- and 4-month lead predictions (Figure 8(b),(d),(f)) in the POST period. Moreover, the MME predictions using both lead times successfully predict the anomalously weakened winter monsoon from Sumatra to southern Japan. However, the observed anomalously wet conditions over SPCZ are not correctly simulated. During the PRE period, the observed dipole of anomalously wet and dry conditions over the equatorial western and central Pacific is not well represented in 1- and 4-month lead MME predictions. There are further limitations in predicting the rainfall anomalies over Indian Ocean, showing the dipole mode at both lead times.

Forecast skills for regional impacts: performance of MME versus performance of individual models

Previous studies have demonstrated that the ENSO is the major predictability source for regional climate forecasts (Wang *et al.* 2008, 2009; Lee *et al.* 2010, 2011b; and many others). Thus, it is important that coupled models are able to capture the regional impacts of ENSO. In order to quantify the skills of the MME in predicting the impacts of the two types of ENSO at 1- and 4-month lead times, we present (Figure 9) the prediction skills of the MME and six individual models relating to the regional impact, for regressed rainfall. These are based on the first two leading EOF modes of the observed and predicted SSTA at 1- and 4-month lead times over the five different regions, namely: the Tropics (30S–30N, 0–360E), Australasia (45S–10S, 110E–180E), East Asia (20N–60N, 90E–150E), North America (20N–60N, 140W–

50W), and tropical South America (15S–10N, 80W–35W). The mean of the prediction skills of the individual models is also calculated. As indicted in Figure 9, at a 1-month lead time the predictive skills of the MME are significantly better in predicting the canonical ENSO-associated impacts, compared with the impacts of the second type of ENSO, (except for East Asia). Specifically, the pattern correlation coefficient for rainfall associated with the canonical ENSO reaches approximately 0.6 for these four regions during the two periods. In contrast, in East Asia, a ENSO Modoki-associated impacts is better predicted at a 4-month lead. In general, the 4-month lead MME prediction for rainfall anomaly exhibits a poorer performance than the 1-month lead MME predictions. However, in this study, the skills for the 4-month lead MME predictions are comparable to those of the 1-month MME predictions for the five above-mentioned regions. As shown in Figure 9, better prediction skills are evident in the POST period than in the PRE period.

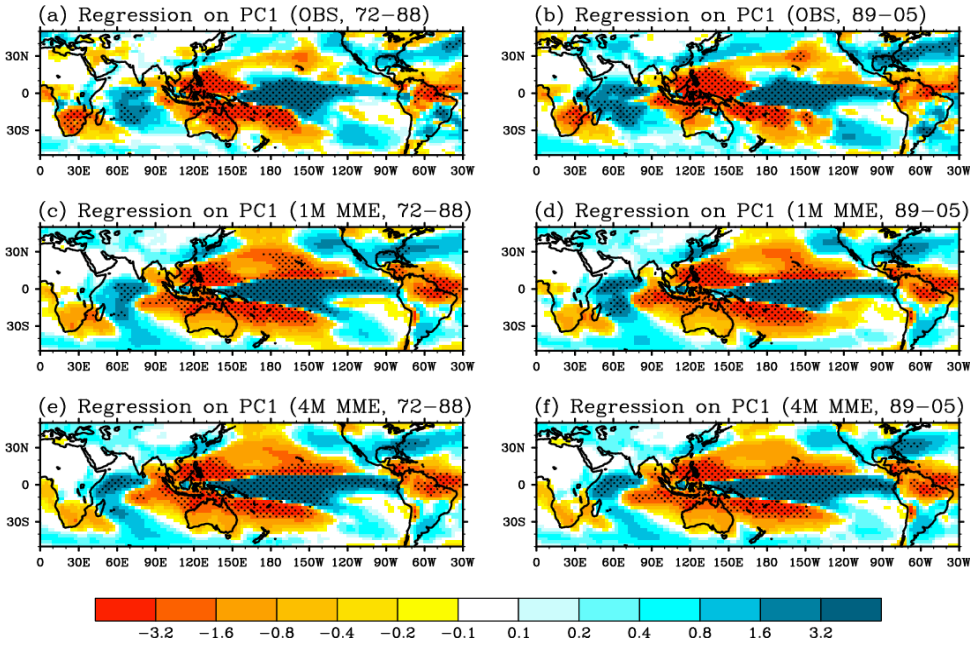

Figure 7 Regression patterns of observed rainfall anomalies based on PC1 time series (see Fig. 4) of the first EOF mode for observed sea surface temperature anomalies in the PRE period (a) and the POST period, (b). (c) and (d) and (e) and (f) are the same as (a) and (b), except for the MME prediction at a 1- and 4-month lead time, respectively. The stippled areas represent significant regression coefficients at the 95% confidence level.

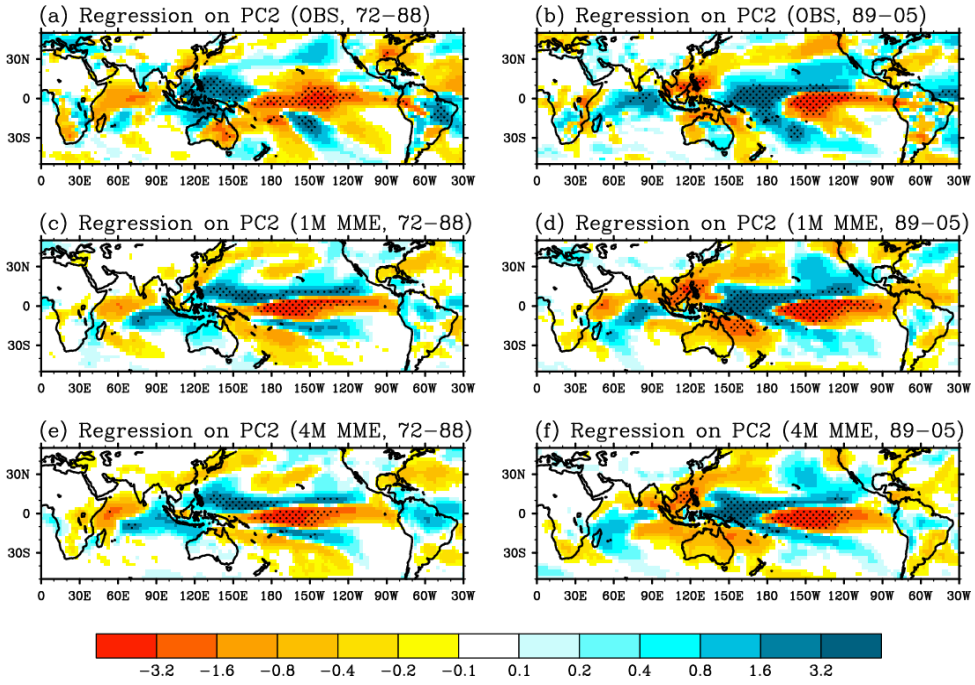

Figure 8 Same as Figure 7, but representing the PC2 time series.

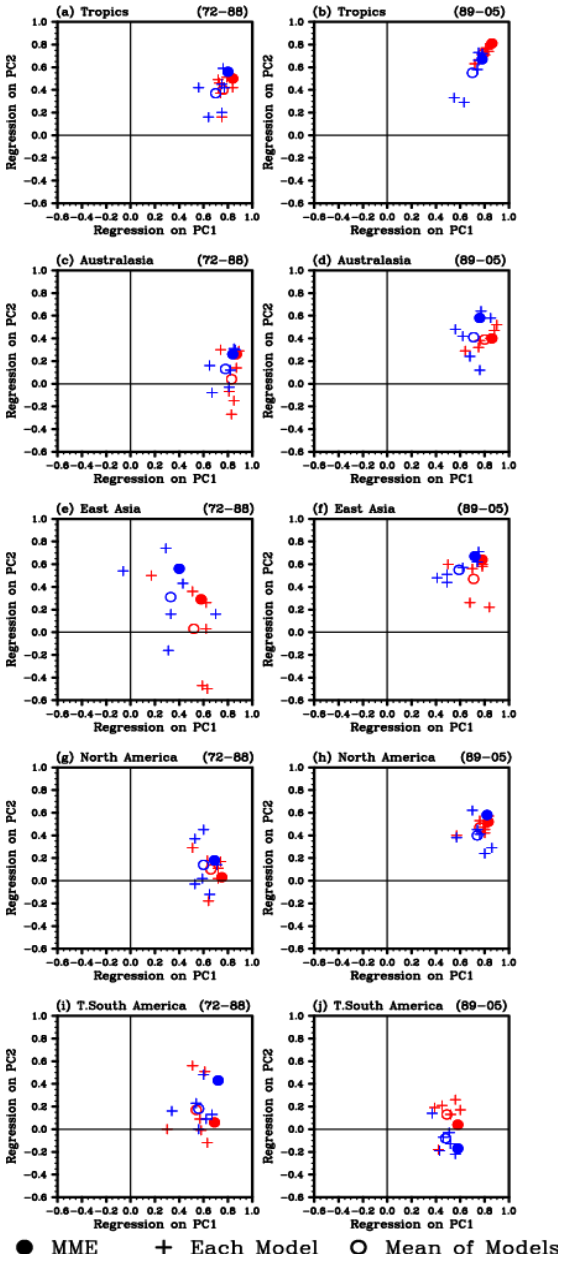

Figure 9 Distribution of the pattern correlation coefficients between regressed patterns of observation and model simulations on each time series of the first two EOF modes for observed and predicted SSTAs at 1-month (red) and 4-month (blue) lead time over the five regions of: the Tropics (30°S–30°N, 0–360°E), Australasia (45°S–10°S, 110°E–180°E), East Asia (20°N–60°N, 90°E–150°E), North America (20°N–60°N, 140°W–50°W), and tropical South America (15°S–10°N, 80°W–35°W). The left panels represent the PRE period and the right panels represent the POST period.

4. CONCLUSION

The purpose of this work was to assess the ability to predict the decadal change of tropical Pacific SST variability during the boreal winter, and also to document the skills of a coupled MME and single models in predicting the respective climate impacts of two types of ENSOs, at a lead time of 1- and 4-months.

The current work demonstrates that, from an EOF analysis of the tropical Pacific SST, the coupled MME prediction has reasonably good skills in simulating the decadal changes of two types of ENSO events, (represented by EOF1 and EOF2). The spatial pattern correlations between the observation and the MME prediction at a 1- and 4-month lead time are 0.94 for the first mode of EOF analysis during both time periods, (even though the total variance of EOF1 is much larger than that of the observation). In the variability of the second mode, the pattern correlations at a 1(4)-month lead time are 0.83(0.81) for the PRE period, while for the POST period the pattern correlation at 1-month lead time is slightly increased to 0.88. However, the total variance associated with the EOF2 is slightly under predicted. At a 4-month lead, the variance explained by the predicted EOF2 is almost 30% (54%) less than that off the observations for the PRE(POST) period. The PC time series for the observed and for the predicted MME are reasonably well correlated for both periods at a 1- and 4-month lead time, indicating an exceptionally statistically-significant confidence level of 99% from the two-tailed Student's t-test.

When evaluating the local climate predictability from the decadal change of tropical Pacific SST variability for the two periods, the MME prediction fairly successfully captures the major features of rainfall anomalies (such as the strong winter monsoon over East Asia, the severe drought condition over Australia, the wet climate over the whole area of USA, and the anomalously dry condition over South America associated with the canonical ENSO). For a regional impact (using the second mode of Tropical SST variability for the recent period), the MME successfully simulates the severe dry conditions over Maritime continents and East Asia for both a 1- and 4-month lead time. However, there are limitations in predicting the exact rainfall conditions for the PRE period; showing unrealistic rainfall anomalies

over the Indian Ocean, equatorial western and the central Pacific at both a 1- and 4-month lead time.

It is evident that further development of higher resolution coupled models with improved dynamical and physical processes, and further improvement in the data assimilation methods is needed to improve the skills in adequately predicting the two phenomena and their teleconnections within a seasonable lead time.

Although we used a simple composite method to form the MME in this study, the application of a variety of statistical MME methods (Krishnamurti *et al.* 2000; Yun *et al.* 2005; Kug *et al.* 2008) could also be useful in obtaining a better prediction of the two phenomena. In addition, the climate filter method (Lee *et al.* 2011a), which separates better performing models using the relative dynamical diagnostic performance within the model itself, may contribute to further improving the seasonal prediction skills of the teleconnections from the tropical Pacific.

REFERENCES

Ashok, K., Nakamura, H., and Yamagata, T. (2007). Impacts of ENSO and IOD events on the Southern Hemisphere storm track activity during austral winter, J. Climate, 20, 3147-3163.

Ashok, K., Iizuka, S., Rao, S.A., Saji, N.H., Lee, W.J. (2009b). Processes and boreal summer impacts of the 2004 El Niño oModoki: an AGCM study. Geophys Res Lett 36:L04703. doi:10.1029/2008GL036313

Ashok, K., Tam, C.Y., Lee, W.J. (2009a). ENSO Modoki impact on the Southern Hemisphere storm track activity during extended austral winter. Geophys Res Lett 36:L12705. doi:10.1029/2009GL038847

Balmaseda, M.A., Vidard, A., and Anderson, D. (2008). The ECMWF ORA-S3 ocean analysis system. Monthly Weather Review 136:3,018–3,034.

Cai, W., Cowan, T. (2009). aLa Niña Modoki impacts Australia autumn rainfall variability. Geophys Res Lett 36:L12805. doi:10.1029/2009GL037885

Chen, M., Xie, P., Janowiak, J. E., and Arkin, P. A., (2002). Global Land Precipitation: A 50-yr Monthly Analysis Based on Gauge Observations, J. of Hydrometeorology, 3, 249-266

Collins, W. J., Bellouin, N., Doutriaux-Boucher, M., Gedney, N., Hinton, T., Jones, C.D., Liddicoat, S., Martin, G., O'Connor, F., Rae, J., Senior, C., Totterdell, I., Woodward, S., Reichler, T., Kim, J., Halloran, P.: Evaluation of the HadGEM2 model. Hadley Centre Technical Note HCTN 74, Met Office Hadley Centre, Exeter, U.K., http://www.metoffice.gov.uk/learning/library/publications/science/climate-science, 2008

Diaz, H.F., Hoerling, M.P., Eischeid, J.K. (2001). ENSO variability, teleconnections and climate change. Int J Climatol 21:1845–1862

Donguy, J.R., Dessier, A. (1983). El Niño-like events observed in the tropical Pacific. Mon Weather Rev 111:2136–2139

Fu, C., Diaz, H., Fletcher, J. (1986). Characteristics of the response of sea surface temperature in the central Pacific associated with warm episodes of the Southern Oscillation. Mon Weather Rev 114:1716–1739

Graham, N. E., (1992). Decadal scale climate variability in the 1970s and 1980s: observations and model results: decadal-to-century time scales of climate variability. Academic, New York.

Graham, N. E., (1994). Decadal scale variability in the tropical and North Pacific during the 1970s and 1980s: Observations and model results. Climate Dyn., 10, 135–162.

Hare, S. R., and Mantua, N. J., (2000): Empirical evidence for North Pacific regime shifts in 1977 and 1989. Prog. Oceanogr., 47, 103–145.

Hendon, H.H., Lim, E., Wang, G., Alves, O., Hudson, D. (2009). Prospects for predicting two flavors of El Nino. Geophys Res Lett 36:L19713. doi:10.1029/2009GL040100

Hollowed, A. B., Hare, S. R., and Wooster, W. S., (2001). Pacific basin climate variability and patterns of northeast Pacific marine fish production. Prog. Oceanogr., 49, 257–282.

Jeong, H.-I., Lee, D.Y., Ashkok, K., Ahn, J.-B., Lee, J.-Y., Luo, J.-J., Schemm, J.-K., Schemm, E., Hendon, H. H., Braganza, K., Han, Y.-G., (2012). Assessment of the APCC coupled MME suite in predicting the distinctive climate impacts of two flavors of ENSO during boreal winter. Clim Dyn. 39:475-493.

Kalnay, E., and co-authors. (1996). The NCEP/NCAR 40-Year Reanalysis Project. Bull. Amer. Meteor. Soc., 77, 437–471

Kang, H., and co-authors. (2009). Statistical Downscaling of Precipitation in Korea Using Multimodel Output Variables as Predictors, Mon. Weather Rev., 137, 1928-1938

Kao, H.Y., Yu, J.Y. (2009). Contrasting eastern-Pacific and central-Pacific types of ENSO. J Clim 22:615–632. doi:10.1175/2008JCLI2309.1

Kug, J.S., Ahn, M.S., Sung, M.K., Yeh, S.W., Min, H.S., Kim, Y.H. (2010). Statistical relationship between two types of El Niño events and climate variation over the Korean Peninsula. Asia Pac J Atmos Sci 46:467–474. doi:10.1007/s13143-010-0027-y

Kug, J.S., Jin, F.F., An, S.I. (2009). Two types of El Niño events: cold tongue El Niño and warm pool El Niño. J Clim 22:1499–1515

Larkin, N.K., Harrison, D.E. (2005a). On the definition of El Niño and associated seasonal average U.S. weather anomalies. Geophys Res Lett 32:L13705. doi:10.1029/2005GL022738

Larkin, N.K., Harrison, D.E. (2005b). Global seasonal temperature and precipitation anomalies during El Niño autumn and winter. Geophys Res Lett 32:L16705. doi:10.1029/2005GL022860

Lee, D.Y., Ashok, K., Ahn, J.-B. (2011). Toward enhancement of prediction skills of multimodel ensemble seasonal prediction: A climate filter concept. Journal of Geophysical Research 116: D06116, DOI:10.1029/2010JD014610

Lee, D. Y., C.-Y. Tam, and C.-K. Park (2008), Effects of multicumulus convective ensemble on East Asian summer monsoon rainfall simulation, J. Geophys. Res., 113, D24111, doi:10.1029/2008JD009847

Lee, J.-Y., Wang, B., Kang, I.-S., and Shukla, J. S. *et al.*, (2010). How are seasonal prediction skills related to models performance on mean state and annual cycle? Clim. Dyn, 35, 267-283.

Lee, S. S., Lee, J.-Y., Wang, B., K.-J. Ha, Wang., Jin, F.-F.; Straus, D.M., and Shukla, J., (2012). Interdecadal changes in the storm track activity over the North Pacific and North Atlantic. Clim. Dyn, 39, 313-327.

Lee, W.-J., and co-authors. (2009). APEC Climate Center for Climate Information Services, APCC 2009 Final Report (Available at http://www.apcc21.net/activities/activities 03_01. php).

Lim E.P., Hendon, H.H., Hudson, D., Wang, G., Alves, O. (2009). Dynamical forecast of inter–El Nino variations of tropical SST and Australian spring rainfall. Mon Weather Rev 137:3796–3810. doi:10.1175/2009MWR2904.1

McPhaden, M.J. (1999). Genesis and evolution of the 1997–1998 El Nin˜o. Science 283:950–954

Mo, K.C. (2010). Interdecadal modulation of the impact of ENSO on precipitation and temperature, over the United States. J Clim 23:3639–3656. doi:10.1175/2010JCLI3553.1

Nitta, T., and Yamada, S., (1989). Recent warming of tropical sea surface temperature and its relationship to the Northern Hemisphere circulation. J. Meteor. Soc. Japan, 67, 375–383.

Peng, P., Kumar, A., Kumar, H., van den Dool, and Barnston, A. G., (2002). An analysis of multimodel ensemble predictions for seasonal climate anomalies, J. Geophys. Res. 107(D23), 4710.

Pradhan, P.K., Preethi, B., Ashok, K., Krishnan, R., Sahai, A.K. (2011). Modoki, Indian Ocean Dipole, and western North Pacific typhoons: Possible implications for extreme events. J Geophys Res 116:D18108. doi:10.1029/2011JD015666

Ratnam, J.V., Behera, S.K., Masumoto, Y., Takahashi, K., Yamagata, T. (2010). Pacific Ocean origin for the 2009 Indian summer monsoon failure. Geophys Res Lett 37:L07807. doi: 10.1029/2010GL042798

Ropelewski, C.F., Halpert, M.S. (1987). Global and regional scale precipitation patterns associated with the El Niño/Southern Oscillation. Mon Weather Rev 115:1606–1626

Ropelewski, C.F., Halpert, M.S. (1989). Precipitation patterns associated with the high index phase of the Southern Oscillation. J Clim 2:268–284

Saji, N.H., Yamagata, T. (2003). Possible impacts of Indian Ocean dipole mode events on global climate. Clim Res 25:151–169

Salas-Mélia, D. (2002). A global coupled sea ice-ocean model. Ocean Modelling 4, 137-172.

Smith, Thomas M., Richard, W. Reynolds, Thomas, C. Peterson, Lawrimore, J. (2008). Improvements to NOAA's Historical Merged Land–Ocean Surface Temperature Analysis (1880–2006). J. Climate, 21, 2283–2296.

Stockdale, T.N., Anderson, D.L.T., Balmaseda, M.A., Doblas-Reyes, F.J., Ferranti, L., Mogensen, K., Palmer, T.N., Molteni, F., Vitart, F. (2011). ECMWF seasonal forecast system 3 and its prediction of sea surface temperature. Clim Dyn. doi:10.1007/s00382-010-0947-3

Tanaka, H. L., Kanohgi, R., and Yasunari, T. (1996). Recent abrupt intensification of the northern polar vortex since 1988. J. Meteor. Soc. Japan, 74, 947–954.

Taschetto, A.S., England, M.H. (2009). El Niño Modoki impacts on Australian rainfall. J Clim 22:3167–3174. doi:10.1175/2008JCLI2589.1

Trenberth, K. and Hurrell, J. (1994). Decadal atmosphere-ocean variations in the pacific. Cli. Dyn., 9, 303-319.

Trenberth, K.E., Stepaniak, D.P. (2001). Indices of El Niño evolution. J Clim 14:1697–1701

Trenberth, K.E., Smith, L. (2009). Variations in the three dimensional structure of the atmospheric circulation with different flavors of El Niño. J Clim 22:2978–2991. doi:10.1175/2008JCLI2691.1

Turner, AG, Inness, P.M., Slingo, J.M. (2007). The effect of doubled CO2 and model basic state biases on the monsoon-ENSO system. II: changing ENSO regimes Q J Roy Meteor Soc 133(Part A): 1159–1173

Walsh, J. E., Chapman, W. L., and Shy, T. L., (1996). Recent decrease of sea level pressure in the central Arctic. J. Climate, 9, 480–486.

Wang, B., (1995). Interdecadal changes in El Niño onset in the last four decades. J. Climate, 8, 267-285.

Wang, B., Yang, J., and Zhou, T., (2008). Interdecadal changes in the major modes of Asian-Australian monsoon variability: Strengthening relationship with ENSO since the late 1970s. J. Climate, 21, 1771-1789.

Wang, B., Lee, J.Y., Kang, I. S., Shukla, J., Park, C. K., Kumar, A., Schemm, J., Cocke, S., Kug, J. S., Luo, J. J., Zhou, T., Wang, B., Fu, X., Yun, W.T., Alves, O., Jin, E.K., Kinter, J., Kirtman, B., Krishnamurti, T., Lau, N. C., Lau, W., Liu, P., Pegion, P., Rosati, T., Schubert, S., Stern, W., Suarez, M., Yamagata, T. (2009). Advance and prospectus of seasonal prediction: assessment of the APCC/CliPAS 14-model ensemble retrospective seasonal prediction (1980–2004). Clim Dyn 33:93–117

Wang, B., Lee, J. Y., Kang, I. S., Shukla, J., Kug, J. S., Kumar, A., Schemm, J., Luo, J. J., Yamagata, T., Park, C. K. (2008). How accurately do coupled climate models predict the leading modes of Asian-Australian monsoon interannual variability? Clim Dyn 30:605–619

Wang, G., Hendon, H. H. (2007). Sensitivity of Australian rainfall to inter-El Niño variations. J Clim 20:4211–4226

Watanabe, M., and Nitta, T., (1999). Decadal changes in the atmospheric circulation and associated surface climate variations in the Northern Hemisphere winter. J. Climate, 12, 494–510.

Weisheimer, A., Doblas-Reyes, F. J., and Palmer, T. N. *et al.,* (2009). Ensembles: A new multi-model ensemble for seasonal-to-annual predictions-skill and progress beyond Demeter in forecasting tropical Pacific SSTs. Geo Res Lett., 36, L21711.

Weng, H., Ashok, K., Behera, S.K., Rao, S.A., Yamagata, T. (2007). Impacts of recent El Niño Modoki on dry/wet conditions in the Pacific rim during boreal summer. Clim Dyn 29:113–129

Weng, H., Behera, S.K., Yamagata, T. (2009). Anomalous winter climate conditions in the Pacific rim during recent El Niño Modoki and El Niño events. Clim Dyn 32:663–674. doi:10.1007 / s00382-008-0394-6

Xie, S., Du, Y., Huang, G., and X. Z. *et al.* (2010b): Decadal shift in El Niño influences on indo-western pacific and east Asian climate in the 1970s. J. Climate, 23, 3352-3368.

Yasunaka, S., and Hanawa, K., (2003). Regime shifts in the Northern Hemisphere SST field: Revisited in relation to tropical variations. J. Meteor. Soc. Japan, 81, 415–424.

Yeh SW, Kug JS, Dewitte B, Kwon MH, Kirtman BP, Jin FF (2009) El Niño in a changing climate. Nature 461:511–514. doi: 10.1038/nature08316

Yeh, S-W, Y. Kang, Y. Noh, and A. Miller, 2011: The North Pacific climate transitions of the winters of 1976/77 and 1988/89. J. Climate. 24, 1170-1183.

Yu, J.Y., Kao, H.K. (2007). Decadal changes of ENSO persistence barrier in SST and ocean heat content indices: 1958–2001. J Geophys Res 112:D13106. doi:10.1029/2006JD007654

Yu, J.Y., Kim, S.T. (2010). Three evolution patterns of Central-Pacific El Nin˜o. Geophys Res Lett 37:L08706. doi:10.1029/2010GL042810

Zhang, Y., Wallace, J., and Battisti, D. (1997). ENSO-like interdecadal variability: 1900-93. J. Climate, 10, 1004-1020.

APCC TECHNICAL REPORT 2012-01

- Application of Bayesian Model Averaging on Multi-Model Ensemble Seasonal Prediction
- Decadal Change of Variability and Predictability of Two Types of ENSO
- Assessment of Relationship between EL Nino and Indian Summer Monsoon Rainfall
- Long-lead MME Extreme Drought Prediction
- Assessment of APCC Multi-Model Ensemble Predictions

APEC Climate Center

12, Centum 7-ro, Haeundae-gu, Busan 612-020,
Republic of Korea
Tel: +82-51-745-3900 Fax: +82-51-745-3949
www.apcc21.org

비매품
9 788997 333363 94500
ISBN 978-89-97333-36-3
ISBN 978-89-97333-35-6 (세트)